ELSEVIER

Journal of Nuclear Materials 280 (2000) 56–72

journal of nuclear materials

www.elsevier.nl/locate/jnucmat

On the behaviour of intragranular fission gas in UO_2 fuel

Pekka Lösönen *

Orkoniitynkatu 9 A 12, 53850 Lappeenranta, Finland

Received 23 November 1998; accepted 23 February 2000

Abstract

Data obtained from the literature concerning the behaviour of intragranular gas in sintered LWR UO_2 fuel are reviewed comprehensively. The characteristics of single gas atoms and bubbles, as a function of irradiation time, temperature, fission rate and burn-up are described, based on the reported experimental data. The relevance of various phenomena affecting gas behaviour is evaluated. The current status of modelling of the behaviour of intragranular gas is considered in light of the present findings. Simple calculations showed that the conventional approximation for the effective diffusion coefficient does not adequately describe the gas behaviour under transient conditions, when bubble coarsening plays a key role in the release. The difference in the release fraction, compared with a more mechanistic approach, could be as large as 30%. A number of recommendations regarding possible defects in the mechanistic approach to modelling of intragranular gas are highlighted. The lack of an effective numerical method for solving the set of relevant non-linear differential equations is shown to be a serious obstacle in implementing the mechanistic models for fission gas release (FGR), in integral fuel performance codes.

1. Introduction

The noble gases xenon and krypton are produced during the fission of uranium and plutonium isotopes in irradiation. Different isotopes of these two heavy elements produce different amounts of the noble gases, and the number of atoms produced depends on the neutron flux spectrum and its density. Roughly 0.26 stable gas atoms are produced for each fission event [1,2].

In irradiation, a fraction of the gaseous fission products generated is released into the free volume of the fuel rods, increasing the pressure inside the cladding. This pressure increase can cause cladding failure and thus contamination of the coolant. An understanding of the fission gas release (FGR) process is therefore essential in optimising fuel usage.

Among the various mechanisms of FGR, diffusional release is the most important for burn-ups below about 50 000 MW d/t U. Other release mechanisms active at low burn-ups, e.g. recoil and knock-out, amongst others, contribute less than 1% to the release of generated gas [3,4]. The release from the porous zone at the rim of the pellets begins to increase with average fuel rod cross-sectional burn-ups of 40 000–50 000 MW d/t U in LWR fuel [5–8]. However, diffusion remains the mechanism with potential for much larger FGR fractions than the other mechanisms combined, even at these high doses [9].

SEM and TEM observations show that FGR in UO_2 fuel takes place through tunnels formed at grain edges and faces during irradiation [10–16]. Diffusion of the gas atoms into the grain boundaries up to the concentration necessary for the formation of tunnels requires a certain incubation time, which is dependent on burn-up [13,17–20]. The mechanisms controlling the behaviour of the gas inside the grains must be known if the FGR process is to be modelled successfully.

Intragranular gas can exist as single atoms in a UO_2 matrix, or may be present in bubbles or in other traps. Both single gas atoms and bubbles experience diffusional motion. A knowledge of the distribution of the gas in the different locations is of prior interest in attempts to understand comprehensively the behaviour of the intragranular gas. In this paper, information on the subject is provided with the help of extensive published

* Present address: 92 route d'Arlon, L-7513 Mersch, Luxembourg. Tel.: +352-4301 32 915.

E-mail address: pekka.loesoenen@cec.eu.int (P. Lösönen).

0022-3115/00/$ - see front matter
PII: S0022-3115(00)00028-3

data. The models used in fuel performance codes are discussed before being summarised, and recommendations made.

2. Single gas atoms

The diffusion coefficient of xenon in oxide nuclear fuels is a function of temperature, stoichiometry and fission rate [21–24]. Turnbull et al. [25] published the following expression for the diffusion coefficient D:

$$D = D_1 + D_2 + D_3, \quad (1)$$

where D_1 represents the intrinsic diffusion coefficient in the absence of irradiation. D_2 and D_3 are functions of fission density, and describe the thermal and athermal effects of irradiation on the diffusion coefficient, respectively [26]. The effect of irradiation exceeds the effect of temperature at temperatures below 800°C in fission rates typical of LWRs [27]. The temperature-independence of the single xenon gas atom diffusion coefficient at low temperatures is illustrated in Fig. 1, in which the diffusion coefficient of Eq. (1) is plotted against reciprocal absolute temperature.

The most favourable sites for Xe atoms in the UO_2 lattice, with regard to thermodynamics, are neutral trivacancies (one uranium vacancy and two oxygen vacancies) in stoichiometric and hypostoichiometric matrices [22,28–31]. In the case of hyperstoichiometric fuel, divacancies or single vacancies are favoured. The calculated distribution of xenon atoms between different lattice positions from reference [29] is plotted as a function of O/U ratio in Fig. 2. The diffusion coefficient for xenon in hypostoichiometric, stoichiometric and hyperstoichiometric UO_2 as a function of reciprocal

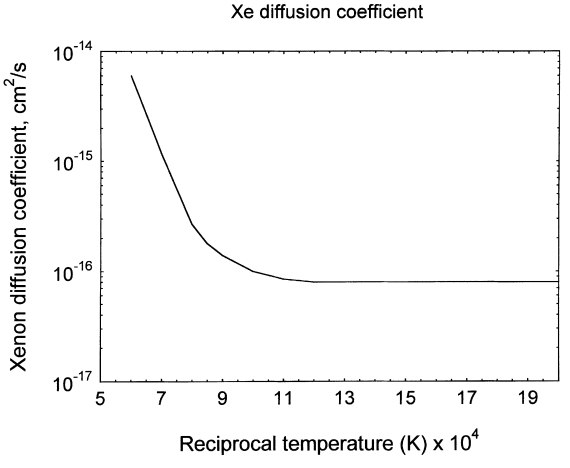

Fig. 1. Xenon diffusion coefficient at a fission rate of 36 W/g in stoichiometric UO_2 as a function of reciprocal temperature [25].

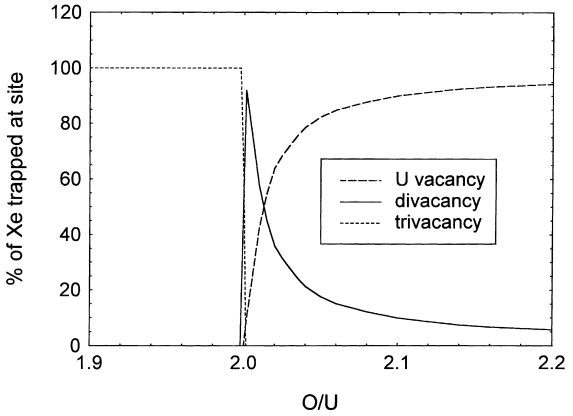

Fig. 2. Calculated distribution of xenon atoms at various matrix positions as a function of O/U ratio in UO_2 at a xenon concentration of 10^{-7} at.% and a temperature of 1400°C [29].

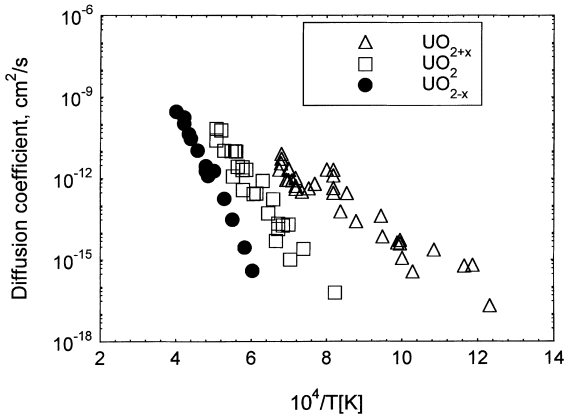

Fig. 3. Measured xenon diffusion coefficient as a function of reciprocal temperature for hypostoichiometric, stoichiometric and hyperstoichiometric UO_{2+x} [32].

temperature is shown in Fig. 3, as presented in reference [32]. Matzke and Lindner have reported that the diffusion coefficient increases in hyperstoichiometric UO_{2+x} with increasing x [33], which may be related to the change in the distribution of xenon atoms at different locations.

The proportion of xenon atoms in divacancies decreases considerably between burn-ups, e.g. 10^{15} and 10^{17} fissions/cm^3 in stoichiometric UO_2 [29]. The diffusion coefficient decreases in the same burn-up range [34], illustrated clearly in Fig. 4, in which the xenon diffusion coefficient in stoichiometric UO_2 at 1400°C is plotted as a function of burn-up, together with the portion of xenon atoms at divacancy sites. The distribution of xenon atoms at different locations inevitably affects the diffusion coefficient, and for stoichiometric fuel the

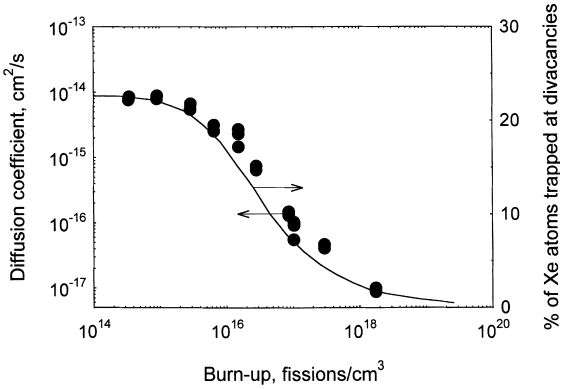

Fig. 4. Measured decrease in the xenon diffusion coefficient in UO_2 [34], and calculated decrease in the proportion of xenon atoms at divacancy sites [29], as a function of burn-up.

distribution is extremely sensitive to the value of x in UO_{2+x}.

In transients, and at high burn-ups, it is possible that oxygen redistribution occurs and the initially stoichiometric fuel becomes hyperstoichiometric [24,35,36]. However, the fission product molybdenum has been shown to buffer the oxygen potential in irradiated oxide fuels even at high burn-ups [37–39]. In normal conditions, the UO_2 fuel can be assumed to be stoichiometric, and use of Eq. (1) is justified. During severe accidents the fuel is most probably hyperstoichiometric, [40] and the diffusion coefficient is larger than that predicted by Eq. (1).

3. Bubbles

3.1. Nucleation and characteristics

The solubility of noble gases in the UO_2 matrix is extremely low. The maximum solubility of Xe has been estimated to be 3×10^{-10} Xe-atoms/U-atom/atm [34,39]. An obvious consequence of the low solubility is the tendency of the moving gas atoms to precipitate into bubbles. The strong tendency of the gas atoms to precipitate into bubbles has been demonstrated for samples implanted with Kr and Xe ions, even at temperatures as low as 300–350°C [41,42]. The nucleation process itself cannot be observed directly, but some interesting observations allow us to draw conclusions from it. Many of the bubbles have been aligned in straight lines in several experiments, where UO_2 samples have been irradiated and analysed [43–47]. The interpretation of these observations is that nucleation takes place in the wake of fission fragments [43,46], and it is often modelled as being proportional to the fission rate [48,49].

Once nucleated, the bubbles become visible in high resolution TEM at a dose of approximately 10^{19} f/cm^3 [50]. The density and the size of the intragranular bubble population are almost independent of the irradiation conditions or burn-up [45,51–57]. Typically, the diameter of the bubbles lies between 1 and 10 nm, and their density is $\sim 10^{17}$ cm^{-3} [43,44,55,57–59], with a narrow size distribution [44,45,54,55,59]. The size of the bubbles increases and the concentration decreases slightly:

1. with increasing temperature,
2. with decreasing specific fission rate, or
3. with increasing burn-up [55,60].

The mean size and the concentration of the bubbles according to Baker [46] are shown in Fig. 5.

At higher burn-ups and/or temperatures a second bubble population is created, which is characterised by a larger mean diameter and a lower density, 20–100 nm and 10^{15} cm^{-3}, respectively [55,59]. These bubbles are often located at dislocations [46,57,59,61]. If the temperature is sufficiently high, these bubbles are surrounded by a very high density of tiny (<10 nm) bubbles, and there exist large areas completely free of bubbles [46,59]. The transitions to this heterogeneous bubble distribution occur at lower temperatures with increasing burn-up. The smallest and largest bubbles are often found in contact with solid inclusions [51,55,57,59,62,63].

Intragranular bubbles become visible in micrographs as a dark ring at a particular temperature, which depends on the burn-up. At the same time, the intergranular bubbles start interlinking, and thermal FGR commences [5,7,64,65]. The size of the intragranular bubbles responsible for the dark ring is ~ 0.1–0.2 μm [6].

When the gas is vented from the grain boundaries through the tunnel network formed, the intragranular

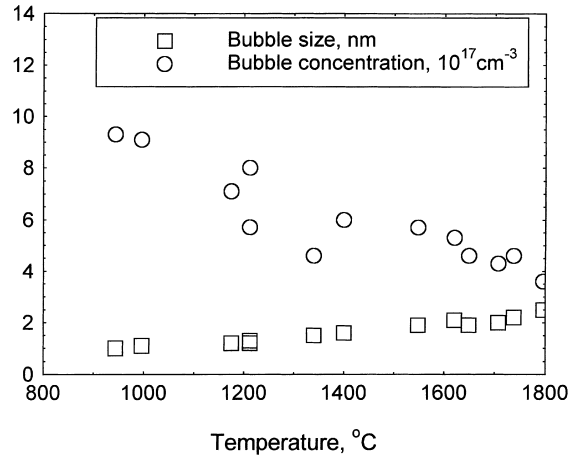

Fig. 5. Density and average size of intragranular bubble population as a function of temperature in irradiated UO_2, as measured by Baker [46].

bubbles first disappear in the vicinity of grain boundaries [66], i.e. the so-called bubble-denuded zones are formed. Finally the intragranular bubble population vanishes completely [5–7,64–66].

A new population of tiny nanometre-size bubbles can be seen at the hottest central parts of the pellets after release is complete [13].

The characteristics of intragranular bubbles in irradiation and in annealing found in the literature are compiled in Table 1.

3.2. Grain growth

FGR is often accompanied by grain growth [5,15,18,67–69]. The moving grain boundaries are believed to be responsible for the bubble-denuded zones near the grain boundaries, since they sweep the bubbles away [70–72]. This would imply that the zones void of bubbles should exist on one side of the grain boundary only. However, the denuded zones are almost always reported to exist on both sides of the grain boundaries [70–74].

The lack of grain growth in many experiments at high temperatures has been explained by the retarding effect of grain boundary bubbles and inclusions on growth [75–77]. Some observations of the hindering effect of precipitates at grain boundaries on grain growth have indeed been reported [78,79].

The grains can grow freely if there are no inclusions or bubbles at the grain boundaries, but once grain growth has started it slows and practically stops rather quickly, because of the precipitating inclusions at the grain boundaries. The observed grain growth associated with the FGR may have occurred after the release, or in the case of a very low burn-up fuel, before the concentration of impurities is sufficient for precipitation. An example of an experiment in Ref. [67], characterised by significant grain growth and very little FGR, supports the possibility of the occurrence of grain growth at low burn-up. However, significant FGR has been reported without grain growth [7,80–82], which is in agreement with the theory that grain growth can occur after major release has occurred [83].

Grain growth and the associated sweeping is not considered a dominating mechanism for the FGR in LWR fuels in normal operation, where the temperatures remain moderate and where the grain boundaries in high burn-up fuel are decorated by solid inclusions or small bubbles.

3.3. Thermodynamic state

The composition and the thermodynamic state of the intragranular bubbles have only been directly measured recently in references [57,84], where results of the examinations of fuel irradiated in several LWRs up to burn-ups between 27 and 48 MW d/kg U were reported. High densities of 1–100 nm gas bubbles and particles existed throughout the spent fuel. Depending on local temperature, the nature of the aggregates changes from 1 to 10 nm bubbles to larger, internally pressurised particles towards interior of the pellet. A population of 20–100 nm bubbles was seen in the centre, or in the centre to mid-radius of the pellets of lowest release, <1.1%. In contrast, in the pellets of higher release (11–18%), larger bubbles were found from the mid-radius to the edge of the pellets.

The 20–100 nm bubbles were found to be of extremely high density, 1.6–3.8 g/cm^3, which is close to the density of solid Xe [57]. The composition of the bubbles or solid particles was approximately Xe–6%Kr, which corresponds roughly to the ratio of the fission yields of the corresponding elements. A consideration of the development of pressure in intragranular bubbles in UO_2 during annealing reveals that the pressure increases with the bubble coarsening process [49]. Thus, the assumption that equilibrium bubbles obey the relation between the pressure, p, and the bubble radius, r:

$$p = \frac{2\gamma}{r} + p_0 \tag{2}$$

must be rejected (γ is the surface energy and p_0 is the hydrostatic pressure). A large excess pressure in inert gas bubbles has also been observed in annealing studies of He-implanted nickel [85]. It is clear that the models must be able to predict the excess pressure in intragranular bubbles.

3.4. Bubble growth and shrinkage

As stated above, the size of the nanometre-scale bubbles tends to increase, and their density tends to decrease with increasing temperature. Apart from the appearance of the larger 10–100 nm bubbles under steady-state conditions, coarsening of the bubbles is particularly noticeable in transients [59].

Possible mechanisms affecting the bubble size in transients, as well as under steady-state conditions, are:

- dislocation loop punching,
- resolution,
- absorption of gas atoms and vacancies,
- migration and coalescence, and
- Ostwald ripening.

The mechanisms are described below, from the viewpoint of their relevance to modelling the behaviour of LWR fuel. To be precise, one should distinguish between the growth of an individual bubble and the coarsening of the bubble population. Migration and coalescence, as well as Ostwald ripening, are coarsening processes that cause the mean size of the bubbles to increase. Absorption of gas atoms and vacancies, and dislocation loop punching, are both growth mechanisms

Table 1
Experimental data for intragranular bubbles in oxide fuels in irradiation

No.	Ref.	Bubble size (nm)	Bubble density ($cm^{-3} \times 10^{17}$)	Burn-up (MW d/t U)	Temperature (°C)	Fission rate ($cm^{-3}\ s^{-1} \times 10^{13}$)	I/A[a]	Homog. (HO), heterog. (HE), align lines (LI)	SEM, TEM, replica	Remarks
1	[110]	50	–	10 000	200, 1000–1500	–	I–A–I	–	Replica	Many bubbles associated with solid inclusions, re-irradiation destroys <100 nm bubbles, gradual resolution seen for larger bubbles
2	[44]	2.8	1.18	1259	1580	0.68	I	LI	TEM	Relatively narrow size distribution
3	[44]	2.6	1.24	1259	1570	0.68	I	LI	TEM	
4	[44]	2.4	1.32	1259	1510	0.68	I	LI	TEM	
5	[44]	2.3	1.83	1259	1470	0.68	I	LI	TEM	
6	[44]	2.0	2.46	1259	1425	0.68	I	LI	TEM	
7	[44]	2.0	2.90	1259	1270	0.68	I	LI	TEM	
8	[44]	1.9	3.30	1259	1060	0.68	I	LI	TEM	
9	[44]	1.8	3.50	1259	980	0.68	I	LI	TEM	
10	[44]	1.7	3.80	1259	860	0.68	I	LI	TEM	
11	[43,50]	0.8	3.3	708	785	0.415–0.26	I	LI	SEM	At $T > 700$°C bubbles are in straight lines
12	[43,50]	0.95	3.0	708	870	0.415–0.26	I	LI	SEM	0.8 nm resolution limit
13	[43,50]	1.05	2.9	708	900	0.415–0.26	I	LI	SEM	
14	[43,50]	0.85	3.4	1416	775	0.259–0.5	I	LI	SEM	
15	[43,50]	0.90	3.2	1416	825	0.259–0.5	I	LI	SEM	
16	[43,50]	0.95	3.0	1416	850	0.259–0.5	I	LI	SEM	
17	[43,50]	1.0	2.9	1416	860	0.259–0.5	I	LI	SEM	
18	[43,50]	1.05	2.7	1416	875	0.259–0.5	I	LI	SEM	
19	[43,50]	1.03	2.6	1416	880	0.259–0.5	I	LI	SEM	
20	[43,50]	0.87	2.6	794	775	0.58–0.642	I	LI	SEM	
21	[43,50]	1.05	2.0	794	950	0.58–0.642	I	LI	SEM	
22	[43,50]	1.25	1.5	794	1075	0.58–0.642	I	LI	SEM	
23	[43,50]	1.3	1.4	794	1110	0.58–0.642	I	LI	SEM	
24	[43,50]	1.35	1.2	794	1200	0.58–0.642	I	LI	SEM	
25	[43,50]	1.35	1.0	794	1250	0.58–0.642	I	LI	SEM	
26	[112]	<2	–	7866	650–850	2.6–3.0	I	–	SEM, TEM	Detection limit 2.5 nm
27	[112]	<2	–	7866	850–1400	2.6–3.0	I	–	SEM, TEM	Some larger, random gas bubbles
28	[112]	4–10	0.12	7866	–	0	A	Mostly HO	SEM, TEM	5–7 s annealing in electron beam

Table 1 (Continued)

29	[112]	4–10	0.24	7866	1500	0	A	Mostly HO	SEM, TEM	Furnace annealing 5 h, some larger bubbles at dislocation lines
30	[46]	1.0	9.3	7866	944	0.94	I	LI, especially at $T > 1000$°C	TEM	At $T > 1700$°C the bubble density increased near grain boundaries and the distribution became non-uniform in grains, large bubbles surrounded by large concentration of smaller bubbles and areas denuded of bubbles
31	[46]	1.1	9.1	7866	996	0.94	I	LI, especially at $T > 1000$°C	TEM	Above 1750°C subgrain network
32	[46]	1.2	7.1	7866	1175	0.94	I	LI, especially at $T > 1000$°C	TEM	
33	[46]	1.2	8.0	7866	1212	0.94	I	LI, especially at $T > 1000$°C	TEM	
34	[46]	1.3	5.7	7866	1212	0.94	I	LI, especially at $T > 1000$°C	TEM	
35	[46]	1.5	4.6	7866	1340	0.94	I	LI, especially at $T > 1000$°C	TEM	
36	[46]	1.6	6.0	7866	1400	0.94	I	LI, especially at $T > 1000$°C	TEM	
37	[46]	1.9	5.7	7866	1548	0.94	I	LI, especially at $T > 1000$°C	TEM	
38	[46]	2.1	5.3	7866	1620	0.94	I	LI, especially at $T > 1000$°C	TEM	
39	[46]	1.9	4.6	7866	1649	0.94	I	LI, especially at $T > 1000$°C	TEM	
40	[46]	2.0	4.3	7866	1707	0.94	I	LI–HE	TEM	
41	[46]	2.2	4.6	7866	1738	0.94	I	LI–HE	TEM	
42	[46]	2.5	3.6	7866	1796	0.94	I	LI–HE	TEM	
43	[46]	1.0	>30	13 962	1400	1.2	I	LI	TEM	
44	[59]	8	0.12	42 140	400–500	Max 1	I	HO	SEM, TEM	Resolution for SEM 5 nm and for TEM 0.5 nm bubbles associated with solid precipitates
45	[59]	7.5	0.19	42 140	1000–1200	Max 1	I	HO	SEM, TEM	Some larger bubbles associated with dislocation lines

Table 1 (Continued)

No.	Ref.	Bubble size (nm)	Bubble density ($cm^{-3} \times 10^{17}$)	Burn-up (MW d/t U)	Temperature (°C)	Fission rate ($cm^{-3}\ s^{-1} \times 10^{13}$)	I/A[a]	Homog. (HO), heterog. (HE), align lines (LI)	SEM, TEM, replica	Remarks
46	[59]	4.5	>1 (local)	42 140	1300–1400	Max 1	I (transient)	HE	SEM, TEM	Inhomogeneous population of large bubbles, 50–500 nm in dislocation lines and small bubbles found in the neighbourhood
47	[55]	2.2	9	23 000	$\leqslant 800$	LWR[b]	I	HO	SEM, TEM	
48	[55]	~2	7	44 000	$\leqslant 800$	LWR	I	HO	SEM, TEM	Above 23 MW d/kg U a new bubble population of 10–20 nm sized appears characterised by increasing bubble density with burn-up
49	[55]	~2	4	83 000	$\leqslant 800$	LWR	I	HO	SEM, TEM	Above 23 MW d/kg U a new bubble population of 10–20 nm sized appears characterised by increasing bubble density with burn-up

[a] Irradiation (I), annealing (A).
[b] Typical PWR or BWR conditions.

for an individual bubble. Resolution of the atoms from the bubbles retards the growth, or may even shrink the bubbles.

3.4.1. Dislocation loop punching

If the pressure inside a bubble induces stresses in the surrounding matrix in excess of the yield strength of the material, the bubble pushes a dislocation into the matrix [86,87]. Traces of this dislocation loop punching have been observed around inert gas bubbles in solids [59,88–91]. The required pressure in the bubbles is [86]

$$p = \frac{2\gamma}{r} + \frac{\mu b'}{2\pi(1-\nu)r_{\mathrm{d}}} \ln \frac{r_{\mathrm{d}}}{r_0}, \tag{3}$$

where the first term on the right-hand side represents the equilibrium pressure, and μ is the shear modulus, ν the Poisson's ratio, b' the Burgers vector, r_0 the core radius of a dislocation (of the order of b'), and r_{d} is the radius of the dislocation loop (of the order of the bubble radius, r).

The validity of this equation has been questioned for bubbles of radius less than $10b'$, and a simpler equation has been proposed [92]

$$p = \frac{2\gamma}{r} + \frac{\mu b'}{r} \tag{4}$$

converging to a value

$$p = \frac{2\mu}{r} + 0.2\mu \tag{5}$$

at large bubble radii.

The bubble volume increases by

$$\Delta V = \pi r^2 b' \tag{6}$$

if the loop punching pressure is exceeded [93].

The thermodynamic state of the gas in bubbles indicates that loop punching is the preferred mode of growth over spontaneous vacancy deposition under constant volume conditions. However, in the unconstrained state, and particularly at high temperatures, vacancy deposition is favoured [94]. Loop punching is certainly a phenomenon of importance in transients, since the pressure inside the bubbles increases considerably with increasing temperature.

A possible mechanism for bubble growth related to dislocation loop punching is the condensation of dislocation loops on the bubbles. A description of this mechanism is given in Ref. [95]. This might be the reason for the observed traces of loop punching around the periphery of the pellets, where the temperature has been far below the plastic transition temperature for UO_2. Possible mechanisms for the necessary local creep induced by displacement damage are discussed in reference [92]. Eq. (5) proved to give good results for inert gas bubbles in metals with a moderate displacement dose, while at higher doses the pressure in the bubbles was considerably lower following damage-induced relaxation.

Under most circumstances, loop punching is the mechanism that also dominates in the creation of self-interstitials and interbubble fracture [96,97].

3.4.2. Absorption of vacancies and gas atoms

The driving force for bubble growth is the pressure inside the bubble and the supersaturation of vacancies in the matrix [94]. The rate of gain of gas atoms of a bubble is [98]

$$\frac{\mathrm{d}N}{\mathrm{d}t} = 4\pi D r C_{\mathrm{g}}, \tag{7}$$

where N is the number of gas atoms in the bubble, D the diffusion coefficient of the gas in the matrix, r the bubble radius, and C_g is the gas concentration in the matrix, if the bubble is assumed a perfect sink. The effect of this on the bubble radius is

$$\frac{\mathrm{d}r}{\mathrm{d}t} = \frac{C_{\mathrm{g}} D \Omega}{r}, \tag{8}$$

where Ω is the volume associated with each gas atom.

In addition, vacancy flow into the bubble changes its radius by [99]

$$\frac{\mathrm{d}r}{\mathrm{d}t} = \frac{D_{\mathrm{s}}}{r}\left(\Delta + \frac{\omega}{kT}\left(p - \frac{2\gamma}{r}\right)\right), \tag{9}$$

where D_{s} is the self-diffusion coefficient characterising the solid, Δ the fractional supersaturation of vacancies in the solid, ω the volume associated with each vacancy, and p is the pressure inside the bubble.

Studies of the thermodynamic state of intragranular bubbles in UO_2 fuel suggest that these equations cannot be used as they are, i.e. the bubbles are not perfect sinks and the vacancy flow is suppressed by scabbing in irradiation. Practically all the gas would be precipitated very quickly in the bubbles, if they were directly applied, even if the irradiation-induced resolution with reasonable parameters would be accounted for [54]. Thermal resolution has been shown to remedy the situation somewhat, if the bubbles are considered overpressurised [49].

3.4.3. Resolution

3.4.3.1. Thermal resolution. There is a continuous flow of both vacancies and gas atoms between the bubbles and the solution. The rate at which the bubbles grow depends on the net flow of vacancies and gas atoms into them [99,100]. If the flow of gas atoms into the bubble is much larger than the vacancy flow, the pressure inside the bubble increases. The increase is suppressed if the gas atom concentration at the bubble surface reaches thermodynamic equilibrium, i.e. the thermal resolution of the atoms from the bubble is equal to the gas flow

into the bubble. The equilibrium gas atom concentration at the bubble surface, C_g^B is given in [100,101] by

$$C_g^B = N_v \exp\left\{ -\frac{E_s}{kT} - \frac{1}{k}\left(\frac{\partial S_g}{\partial N_g}\right)_{T,V} + \frac{\Delta S}{k} - \left(p - \frac{2\gamma}{r}\right)\frac{v\Omega}{kT}\right\}\frac{1}{k}\left(\frac{\partial S_g}{\partial N_g}\right)_{T,V}$$

$$= \frac{9}{2} - \ln\left(\frac{N_G}{V}\Lambda^3\right) - \left\{\frac{2}{1-y} + \frac{1+2y}{(1-y)^2} + \frac{2y}{(1-y)^3}\right\},$$

$$y = \frac{4}{3}\pi r_a^3 \frac{N_G}{V}, \tag{10}$$

where N_v is the number of gas atom sites per unit volume of fuel, E_s the gas atom solution energy, ΔS the solution entropy, p the pressure in a bubble of radius r, γ the surface energy, $v\Omega$ the volume associated with a gas atom in the matrix, k Boltzmann's constant, T the temperature, Λ the entropy parameter, y the reduced density, r_a the radius of the gas atom, N_G the number of gas atoms in a bubble, and V is the volume of the bubble.

The concept takes into account the entropy change of the gas in the bubbles when new gas atoms are introduced. The net flux of gas atoms into a bubble is then

$$\frac{dN_g}{dt} = 4\pi r D_g\left(C_g - C_g^B\right), \tag{11}$$

where D_g is the gas atom diffusion coefficient and C_g is the gas atom concentration in the matrix.

The entropy term in Eq. (10) turns sharply negative at the phase transition of a hard sphere fluid at a reduced density $y = 0.467$ [100]. The gas flow from thermal resolution would encounter a step increase, if the reduced density $y = 0.467$ were exceeded. The net flux from thermal resolution from the bubbles becomes positive if the concentration in the matrix is lower than the equilibrium concentration on the surface of the bubble.

FGR in annealing experiments has been calculated in [102] with the assumptions of an absence of bubble mobility and thermal resolution according to [100]. The vacancy flow from the grain boundaries has been calculated using the corresponding diffusion equation. The results show that uncertainties in the stoichiometry of the fuel affect the vacancy flow and the release fraction crucially. By varying the stoichiometry in a reasonable range, the large differences in the measured release fractions of samples annealed in the same temperature would be predicted. The model includes many parameter values which are not known well. Despite the deficiencies, the model proved capable of predicting the possible effect of thermal resolution on the FGR in transients.

Rest has tested a few gas precipitation models in [103]. The models included intragranular bubble nucleation, irradiation-induced resolution and vacancy diffusion, which were assumed rate-controlling in bubble growth. Thermal resolution was not accounted for, but a model that suppressed the gas precipitation rate with increasing overpressure presented by Ronchi [104] was assessed as an alternative. According to Ronchi's model, the stress field around overpressurised bubbles hinders precipitation. The enhanced FGR in transients could be predicted well with that model. However, the results were compared with the measured release versus time, and no data on the bubble population were available. Nevertheless, even with some deficiencies, the exercise shows that the kinetics of gas precipitation may well depend on bubble overpressurisation effects [103]. Theoretical calculations of the resolution from small under- and overpressurised Xe bubbles in UO_2 show that resolution is much more probable from the overpressurised bubbles [31,105].

The effect of the stress field around an overpressurised bubble on the precipitation of Xe in UO_2 can be questioned if the xenon atoms are assumed to be located mainly in neutral trivacancies, since the volume of a Xe atom is small compared with the volume of a trivacancy. Thus, an atom sitting in a neutral trivacancy generates no strain in the lattice [100].

Evans et al. [106] have questioned the effect of thermal resolution from inert gas bubbles in UO_2. In their experiment, UO_2 samples were implanted with Kr ions and the samples were then annealed. The behaviour of the bubbles was followed using TEM imaging. The gas release was continuously monitored. The increasing mobility of the bubbles with increasing temperature was considered to be an effect of a reduction in overpressure caused by thermal vacancies. The migration of the bubbles was seen to cause bubble coarsening through coalescence. No bubble size shrinkage was observed, which was attributed to the absence of thermal resolution from the overpressurized bubbles. The bubbles swept by a moving grain boundary were not seen on the boundaries, and they were thought to have escaped to the free volume. The absence of bubble shrinkage does not, however, exclude the possibility that thermal resolution could have occurred without bubble shrinkage. This was observed for helium bubbles in silicon [107], where the high vacancy formation energy and low vacancy concentration were associated with the absence of shrinkage of the bubbles. The experiments with thin specimens do not necessarily give results analogous to the annealing of larger samples, because the vicinity of the free surface has been observed to be a much better source of vacancies than a grain boundary [108].

3.4.3.2. Irradiation resolution. Shrinkage or disappearance of gas bubbles in solids has been demonstrated in

irradiation–annealing experiments [109–111]. Resolution induced by irradiation has been found to be an extremely effective means of reducing bubble growth [110–112]. Small bubbles (<20 nm) are prone to disappear with a collision of only a single fission fragment [113]. Larger bubbles shrink gradually [110]. The effect of irradiation-induced resolution on the gas concentration in the bubbles is modelled using the parameter b:

$$b = -\frac{1}{m}\frac{\mathrm{d}m}{\mathrm{d}t}, \tag{12}$$

where m is the number of gas atoms in a bubble irradiated for time, t. A numerical value for b has been determined experimentally in various studies [56,110–112]. At conditions relevant for LWR fuel, the resolution parameter lies in the range between 2×10^{-4} and 4×10^{-4} s^{-1} [56]. The value of b is a function of the fission rate.

The effect of irradiation resolution has been disputed by Ronchi and Elton [114], who claimed that shock waves caused by the fission spikes can scab vacancies and produce voids near the bubbles, if the lattice strain exceeds the mechanical strength of the material [115]. The effect of the scabbing mechanism is explained to disorder the lattice such that the 'destroyed' bubbles are not seen in micrographs. Turnbull and Cornell found indeed that annealing of fuel in which bubbles had been destroyed at low temperature produced reprecipitation of a similar population of bubbles to that existing prior to irradiation [52]. Void platelets of ~ 20 nm diameter have been seen near the surface of irradiated UO_2 [114,116], which is direct evidence of existence of the scabbing mechanism.

The situation with considerable overpressure in the bubbles is achieved if the vacancy flow into the bubbles is not sufficient to relieve the pressure. This is certainly true in annealing transients in UO_2 fuel [49], but it can also happen under steady-state conditions [84]. The low metal self-diffusion coefficients in hypostoichiometric and stoichiometric fuels are thought to be the reason for the slow relief of pressure by vacancy flow into intragranular bubbles [101]. The lack of vacancies is certainly obvious if scabbing of vacancies from the bubbles by fission spike-induced shock waves is accounted for.

Resolution from intragranular bubbles is essential in modelling the behaviour of noble fission gases in irradiation of UO_2 fuel. The theory of interaction of the shock waves with the bubbles provides an explanation for the overpressurisation of the bubbles.

3.4.4. Migration and coalescence

Brownian motion of the bubbles leads to their coalescence and to a gradual increase in the mean bubble size. Migration to grain boundaries leads to a direct increase in the gas concentration on the boundaries. There are three main mechanisms responsible for the migration of the bubbles, namely [63]:

- volume diffusion,
- surface diffusion, or
- evaporation–condensation.

The diffusivities of the bubbles in irradiated fuels are in general much lower than calculated values [117,118], if surface diffusion is assumed to be rate controlling. The reasons for the slow mobility of the bubbles could be inclusions of impurities on the surface of the bubbles [63,119–121], facetting of the bubbles [47,122], non-relaxed atomic forces around very small bubbles [123], attachment to dislocations [124–126], overpressure in the bubbles [127–129], or a large mean jump distance in surface diffusion [121,130].

Solid inclusions accompanying inert gas bubbles effectively inhibit movement of the bubbles [63,118,131]. Therefore the experiments with implanted annealed fuel do not give representative results for the bubble migration in irradiation, because in the case of a lack of solid inclusions their retarding effect on bubble mobility is overlooked.

Diffusion coefficients for inert gas bubbles deduced from experiments with irradiated UO_2 fuel show a maximum at a fuel radius between 1 and 10 nm [127]. The experimental and theoretical maximum at ~ 1550°C is about 10^{-16} cm^2/s. An experiment with irradiated fuel under transient conditions providing a deep temperature gradient gave a diffusion coefficient of the same order of magnitude for 10 nm size bubbles [132]. The measured diffusion coefficients are too low to explain FGR in LWR fuel under normal operation [49,60,100].

Bubble diffusivity along a vacancy gradient near grain boundaries has been the basis of a model for FGR in transient annealing [133]. According to the model, the gas bubbles close to the grain boundary should increase in size compared with the bubbles in the centre of the grains. This has been observed for He bubbles in metals [85] and also for fission gas bubbles in irradiated UO_2 in annealing [55,134]. The conditions in the experiment in [133] do not correspond to irradiation, since the solid inclusions attached to the bubbles inhibiting their movement were not present. The debate about possible bubble migration along vacancy gradients continues [135,136].

3.4.5. Ostwald ripening

Coarsening of gas bubbles by Ostwald ripening occurs through resolution and subsequent re-absorption of the atoms and vacancies into the bubbles [137]. The redissolved gas atoms are absorbed into larger bubbles rather than smaller ones, which gradually shrink.

Coarsening by Ostwald ripening is strongly reduced if the bubbles are overpressurised [129,137]. An adequate supply of vacancies is therefore necessary for

relaxing the overpressure in bubbles in irradiated UO_2 to trigger the Ostwald ripening process. The grain boundaries act as effective sources of thermal vacancies, and in annealing experiments the bubbles close to the boundaries are seen to grow more rapidly than in the bulk material [55,106,138].

Ostwald ripening in the development of the intragranular bubble population in irradiation is most probably not very significant, but in annealing it is certainly not negligible.

4. Discussion

Uncertainty concerning the distribution of gas between bubbles and matrix, as a function of time, temperature, fission rate and gas concentration, appears to be the main obstacle to modelling the behaviour of intragranular gas. Correct release values should be predicted using models based on experimental observations of the corresponding phenomena. A summary of relevant mechanisms is presented in Table 2, together with their references. It is to be noted that only indirect evidence exists for some important phenomena, such as Ostwald ripening and thermal resolution.

Mechanistic modelling of the development of the intragranular bubble population, and the concentration of gas at grain boundaries during time-varying conditions in LWR fuel irradiation, require knowledge of the following models, at the very least:

- resolution from intragranular bubbles,
- resolution from grain boundary bubbles, and
- thermodynamic treatment of the growth of intragranular bubbles.

Also, the development of the bubble structure at elevated temperatures cannot be properly described without an understanding of bubble migration and coalescence. A model for the bubble size distribution would perhaps be necessary to handle transient conditions. Models for bubble nucleation and grain boundary sweeping may also be important.

A model for bubble growth by vacancy and gas atom collection can perhaps predict the observed overpressure in the bubbles, if the vacancy absorption is assumed rate controlling and slow enough. However, the effect of vacancy scabbing by passing shock waves from irradiation spikes is certainly worth considering. The available experimental data also indicate the necessity of employing a bubble growth model by dislocation loop punching, especially in transients.

The behaviour of intragranular gas in fuel performance codes is modelled in various ways. The codes can be divided into two categories: integral codes and codes dedicated only to FGR – so-called separate effects models. The models in integral codes are usually relatively simple, since the codes are required to calculate many other phenomena, too. However, codes dedicated solely to the FGR calculations may even contain fuel temperature as an input parameter.

The models can also be classified by their fundamental approach to bubble/single gas atom diffusion:

- no migration of bubbles, only single gas atom diffusion,
- diffusion of both single gas atoms and bubbles, and
- only bubble migration considered.

Models in the last category are not evaluated, since in the LWR fuel single gas atom diffusion dominates up to 1800°C [139].

The codes with single gas atom diffusion are based almost invariably on the formalism of Speight [140], who presented his theory on gas atom trapping and resolution in spherical grains with the solution equivalent to that of Booth's, if the gas atom diffusion coefficient D is replaced by the effective diffusion coefficient D':

$$\begin{aligned} \frac{\partial c}{\partial t} &= \beta + D\nabla^2 c - gc + bm, \\ \frac{\partial m}{\partial t} &= gc - bm \\ D' &= \frac{Db}{b+g}, \end{aligned} \tag{13}$$

Table 2
Phenomena concerning the behaviour of intragranular gas in sintered UO_2 fuel in LWR irradiation

Phenomenon	Direct evidence	Indirect evidence
Bubble precipitation	Yes [43,44,55,57–59]	
Linear nucleation of bubbles	No	Yes [43–47]
Slow mobility of bubbles	Yes [117,118,132]	No
Migration and coalescence of bubbles	Only in annealing [106]	Only in annealing [55]
Dislocation loop punching	No	Yes [59]
Bubble over pressurisation (vacancy starvation)	Yes [57,84]	Yes [49]
Irradiation resolution	Yes [109–111]	No
Scabbing of vacancies	Yes [114,116]	Yes [52]
Thermal resolution and Ostwald ripening	No	Yes [49,55]
Grain boundary sweeping	Only in annealing [106]	No

where c is the concentration of gas in solution, β the gas generation rate, g the probability per second of a gas atom in solution being captured by a bubble, b the probability per second of a gas atom in a bubble being re-dissolved, and m is the amount of gas in the bubbles per unit volume.

Further, the model structure presented in [141] concerning bubble nucleation and destruction has been used as the basis for many codes [48,142–146]. The variations in the codes appear of course in the method of solving the equations, and in the slightly different form of the parameters g and b. Treatments of resolution from grain boundaries, bubble nucleation and grain growth are also different. The results of a survey of models in codes available in the open literature are shown in Table 3. The data are never exactly current, because development work on the codes is a continuous process.

Scabbing and dislocation loop punching are not modelled in the codes listed in Table 3, nor is the bubble size distribution included. Under transient conditions the radial profile of the total gas concentration, and its distribution between the bubbles and the matrix, is also missing. The natural reason for the absence of these important features in the codes is the rapidly increasing computing time and the need for storage of many variables when shifting towards the direction of more detailed models. However, no comprehensive estimates of the effect of the simplifications under various conditions on the results were found in the literature. The numerical methods for solving the problems themselves induce contributions to the total error.

The weakness of Speight's concept of the effective diffusion coefficient is that it fails to describe abnormal conditions properly, e.g. conditions in which the fission rate changes drastically, or when the temperature changes in the absence of fission. The results of the simplifications of Speight's model are examined for two simple cases: zero initial concentration and a rectangular initial concentration profile. Speight's solution is compared with a solution in which the development of the bubble radius is accounted for by

$$\frac{\partial R(r,t)}{\partial t} = \Omega\left(\frac{Dc}{R(r,t)} - \frac{bm(r,t)}{4\pi R(r,t)^2 C_b}\right), \tag{14}$$

where R is the bubble radius, C_b the bubble density, and Ω is the volume associated with each gas atom. The gas density in the bubbles is chosen to be 3.4 g/cm^3, which is within the experimentally verified range 1.6–3.8 g/cm^3. The selected gas density gives a value of 6.5×10^{-29} m^3 for Ω. For the case of the rectangular initial concentration profile most of the gas is assumed to be in the matrix at the beginning of the calculation, when the diffusion coefficient is suddenly increased, simulating a rapid transient. The total amount of gas in the grain corresponds to the gas produced up to a burn-up of 25 MW d/kg U under LWR conditions. The values for the other parameters are shown in Table 4.

The set of non-linear partial differential equations is solved by forming first finite-difference approximations from the spatial derivative terms, and applying the four-point Runge–Kutta method with adaptive step size control according to [156]. The grain is divided into 65 radial nodes. The accuracy of the solution is checked against Speight's solution.

The results for the case of zero initial concentration and a rectangular initial concentration profile are shown in Figs. 6 and 7, respectively. Fig. 7 includes an additional curve representing a case in which bubble

Table 3
Phenomena included in fission gas release models[a]

Integral code	GBR	IR	TR	GBS	BN	BD	BG
COMETHE III-J [147]		X		X			
STAV [148]	X	X					
ELESIM [149]				X			
FEMAXI-IV [144]	X	X		X	X		X
FRAPCON-2 [150]	X						
SIERRA [146]	X	X		X	X		X
SINGAR [101,102]		X	X				X
ENIGMA [48,142]	X	X	X	X	X		X
FUTURE [151,152]	X	X	X	X		X	X
Separate FGR models by author							
Kogai [153]				X			
Charles et al. [154]	X	X					
Ronchi and Sakellaridas [155]	X	X				X	X
Hiramoto et al. [48]		X			X	X	X

[a] GBR – grain boundary resolution; IR – trapping and irradiation resolution; TR – thermal resolution; GBS – grain boundary sweeping; BN – bubble nucleation; BD – bubble diffusion; BG – bubble growth.

Table 4
Parameters for the calculation of the release fractions in two cases by applying the bubble precipitation–resolution approach

	Exact solution	Speight's approximation
b	3×10^{-4} s^{-1}	3×10^{-4} s^{-1}
r	5 μm	5 μm
$C_b(r,t)$	5×10^{23} bubbles/m^3	5×10^{23} bubbles/m^3
β	0.26×10^{19} atoms/m^3 s	0.26×10^{19} atoms/m^3 s
Zero initial concentration		
$R(r,0)$	0	1 nm
D	3.028×10^{-19} m^2/s	3.028×10^{-19} m^2/s
Constant initial concentration profile		
$R(r,t_0)$	1 nm	1 nm
D	4.636×10^{-17} m^2/s	4.636×10^{-17} m^2/s
$c(r,t_0)$	1.6936×10^{26} atoms/m^3	1.6936×10^{26} atoms/m^3
$m(r,t_0)$	5.6711×10^{23} atoms/m^3	5.6711×10^{23} atoms/m^3

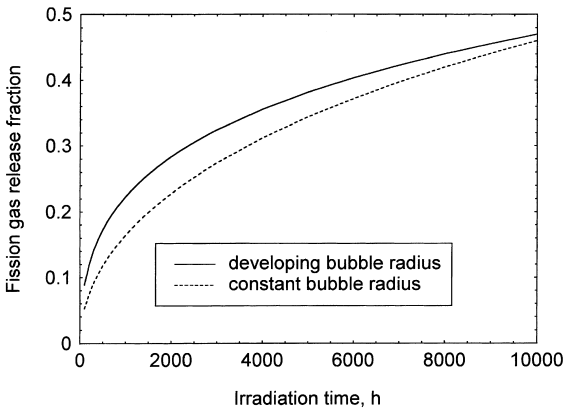

Fig. 6. Calculation of fission gas release from a spherical grain under constant irradiation conditions and zero initial concentration.

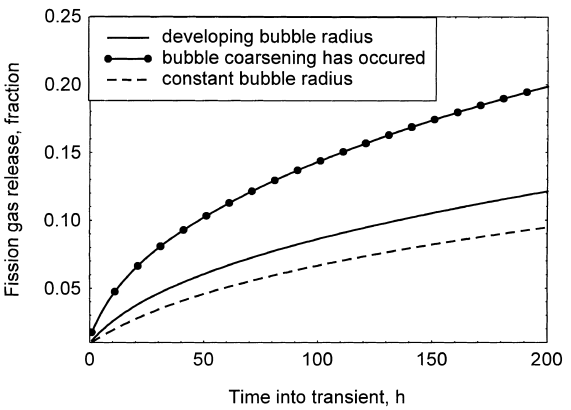

Fig. 7. Calculation of fission gas release from a spherical grain under constant irradiation conditions and a rectangular initial concentration profile.

coarsening has occurred, and the resulting bubble density is only 10% of the original, while the gas density in the bubbles and the gas distribution between the bubbles and the matrix at the beginning of the calculation remain unaltered. The bubble radius is then $10^{1/3}$ times the initial radius.

There is a clear difference in the release fractions between Speight's approach and the more mechanistic model. The relative difference in the release fraction compared with Speight's solution is even up to 30%. The strong effect of the reduced sink strength of the bubble population, caused by its coarsening, on the release rate is very noticeable. Although weaknesses in the current simplified models in integral fuel performance codes are evident, the lack of an effective numerical method for solving the set of non-linear differential equations hinders the implementation of the mechanistic models for FGR in the codes.

5. Summary and recommendations

The behaviour of the intragranular inert gases xenon (and krypton) in irradiation of LWR UO_2 fuel has been reviewed. Experimental data and models reported in the literature have been discussed. Only the behaviour of stable gas was included in the evaluation.

The experimental data revealed the following characteristics of the gas:

1. The gas atom diffusion coefficient is a function of temperature, fission rate, burn-up and stoichiometry.
2. The gas has a tendency to precipitate into bubbles, whose composition is Xe and Kr, lying close to the ratio of their generation rate in fission.
3. The density of the bubble population and the mean size of the bubbles are approximately constant over a relatively wide range of burn-ups and temperatures in LWR fuel.

4. The bubbles are normally overpressurised in irradiation.
5. The mobility of the bubbles is clearly lower than theoretical considerations predict.
6. The bubble population coarsens in transients and in annealing conditions.

The calculations revealed that Speight's widely applied approximation for the effective diffusion coefficient is inadequate in describing the release process under conditions of changing bubble radius. In transients in particular, when pronounced bubble coarsening takes place, the release rate depends strongly on the development of the characteristics of the bubble population.

The following recommendations are made from the reviewed experimental data and from the current status of modelling:

1. A more elaborate thermodynamic approach should be considered for bubble growth, which accounts for the high overpressure observed.
2. A mechanistic approach in modelling the bubble coarsening process should be applied.
3. An effective and accurate numerical method for solving the set of non-linear equations describing the gas behaviour in the grains, including the development of bubble size, should be applied to integral fuel performance codes.

References

[1] Fission Products – Selected Cumulative Chain Yields – Nuclear Reactor Containment Technology – ORNL – NSIC-5, vol. 1, Oak Ridge National Laboratory, Oak Ridge, Tennessee, 1967.
[2] J.W. Harrison, L.M. Davies, J. Nucl. Mater. 27 (1968) 239.
[3] C. Wise, J. Nucl. Mater. 136 (1985) 30.
[4] B.J. Lewis, J. Nucl. Mater. 148 (1987) 28.
[5] C. Forat, B. Blanpain, B. Kapusta, P. Guedeney, P. Permezel, in: Proceedings of a Technical Committee Meeting, Pembroke, Ont., Canada, 28 April – 1 May 1992, IAEA-TECDOC-697, p. 68.
[6] R. Manzel, R. Eberle, in: Proceedings of the International Topical Meeting on LWR Fuel Performance, 21–24 April 1991, Avignon, France, ANS/ENS, p. 528.
[7] J.O. Barner, M.E. Gunningham, M.D. Fresley, D.D. Lanning, in: Proceedings of the International Topical Meeting on LWR Fuel Performance, 21–24 April 1991, Avignon, France, ANS/ENS, p. 538.
[8] F. Lemoine, M. Balourdet, in: Proceedings of the International Topical Meeting on LWR Fuel Performance, Portland, OR, USA, 2–6 March 1997, ANS, p. 693.
[9] R. Manzel, M. Coquerelle, in: Proceedings of the International Topical Meeting on LWR Fuel Performance, Portland, OR, USA, 2–6 March 1997, ANS, p. 693.
[10] J.A. Turnbull, J. Nucl. Mater. 50 (1974) 62.
[11] J.A. Turnbull, M.O. Tucker, Philos. Magn. 30 (1) (1974) 47.
[12] M.O. Tucker, Radiat. Eff. 53 (1980) 251.
[13] M. Mogensen, C.T. Walker, I.L.F. Ray, M. Coquerelle, J. Nucl. Mater. 131 (1985) 162.
[14] M.O. Tucker, R.J. White, J. Nucl. Mater. 87 (1979) 1.
[15] J. Novak, I.J. Hastings, International Topical Meeting on LWR Fuel Performance, 21–24 April 1991, Avignon, France, ANS/ENS.
[16] D.A. Collins, R. Hargreaves, in: J.E. Harris, E.C. Sykes (Eds.), Proceedings of an International Conference on the Physical Metallurgy of Reactor Fuel Elements, Gloucesterhire, UK, 2–7 September 1973, The Metals Society, 1975.
[17] R.G. Bellamy, J.B. Rich, J. Nucl. Mater. 33 (1969) 64.
[18] D. Baron, E. Mafféïs, in: Proceedings of a Specialists' Meeting on Water Reactor Fuel Element Performance Computer Modelling in Bowness-on-Windermere, UK, 9–13 April 1984, p. 425, IWGFPT/19.
[19] C. Bagger, M. Mogensen, in: Proceedings of a Technical Committee Meeting, Pembroke, Ont., Canada, 28 April – 1 May 1992, IAEA-TECDOC-697, p. 38.
[20] W. Wiesenack, in: Proceedings of a Technical Committee Meeting, Pembroke, Ont., Canada, 28 April – 1 May 1992, IAEA-TECDOC-697, p. 118.
[21] W. Miekeley, F.W. Felix, J. Nucl. Mater. 42 (1972) 297.
[22] Hj. Matzke, Radiat. Eff. 53 (1980) 219.
[23] K.N.G. Kaimal, M.C. Naik, A.R. Paul, J. Nucl. Mater. 168 (1989) 188.
[24] B. Grapengiesser, D. Schrire, in: Proceedings of a Technical Committee Meeting, Pembroke, Ont., Canada, 28 April – 1 May 1992, IAEA-TECDOC-697, p. 103.
[25] J.A. Turnbull, R.J. White, C. Wise, in: Proceedings of a Conference on Water Reactor Fuel Element Computer Modelling in Steady State, Transient and Accident Conditions, Preston, UK, 18–22 September 1988, p. 174, IWGFPT/32.
[26] J.A. Turnbull, C.A. Friskney, J.R. Findlay, F.A. Johnson, A.J. Water, J. Nucl. Mater. 107 (1982) 168.
[27] M. Hirai, J.H. Davis, R. Williamson, J. Nucl. Mater. 226 (1995) 238.
[28] R.W. Grimes, in: S.E. Donelly, J.H. Evans (Eds.), Fundamental Aspects of Inert Gases in Solids, Plenum, New York, 1991, p. 415.
[29] S. Nicholl, Hj. Matzke, C.R.A. Catlow, J. Nucl. Mater. 226 (1995) 51.
[30] H. Matzke, J.A. Davies, J. Appl. Phys. 38 (1967) 805.
[31] R.A. Jackson, C.R.A. Catlow, J. Nucl. Mater. 127 (1985) 161.
[32] W. Miekeley, F.W. Felix, J. Nucl. Mater. 42 (1972) 297.
[33] R. Lindner, Hj. Matzke, Z. Naturforsch. A 14 (1959) 582.
[34] J.R. MacEwan, W.H. Stevens, J. Nucl. Mater. 11 (1964) 77.
[35] K. Lassmann, J. Nucl. Mater. 150 (1987) 10.
[36] C.T. Walker, M. Mogensen, J. Nucl. Mater. 149 (1987) 121.
[37] H. Matzke, J. Nucl. Mater. 208 (1994) 18.
[38] S. Nicoll, Hj. Matzke, R.W. Grimes, C.R.A. Catlow, J. Nucl. Mater. 240 (1997) 185.
[39] H. Kleykamp, J. Nucl. Mater. 131 (1985) 221.
[40] J.T. Bittel, L.H. Sjodahl, J.F. White, J. Am. Ceram. Soc. 52 (1969) 445.
[41] J.H. Evans, J. Nucl. Mater. 188 (1992) 222.

[42] H. Matzke, A. Turos, J. Nucl. Mater. 188 (1992) 285.
[43] J.A. Turnbull, J. Nucl. Mater. 38 (1971) 203.
[44] R.M. Cornell, M.V. Speight, B.C. Masters, J. Nucl. Mater. 30 (1969) 170.
[45] R.M. Cornell, J. Nucl. Mater. 38 (1971) 319.
[46] C. Baker, J. Nucl. Mater. 66 (1977) 283.
[47] C. Baker, J. Nucl. Mater. 71 (1977) 117.
[48] K. Hiramoto, K. Miki, M. Nakamura, Nucl. Eng. Design 81 (1984) 395.
[49] R.J. White, in: Proceedings of the International Topical Meeting on Light Water Reactor Fuel Performance, West Palm Beach, FL, USA, 17–21 April 1994, p. 196.
[50] R.M. Cornell, J. Nucl. Mater. 38 (1971) 121.
[51] L.E. Thomas, J. Nucl. Mater. 188 (1992) 80.
[52] J.A. Turnbull, R.M. Cornell, J. Nucl. Mater. 36 (1970) 161.
[53] J.A. Turnbull, R.M. Cornell, J. Nucl. Mater. 37 (1970) 355.
[54] Regional Training Course on the TRANSURANUS Code organised by the IAEA and the European Commission, Joint Research Centre, Institute for Transuranium Elements, 17–21 June 1996, Karlsruhe, Germany.
[55] S. Kashibe, K. Une, K. Nogita, J. Nucl. Mater. 206 (1993) 22.
[56] J.A. Turnbull, R.M. Cornell, J. Nucl. Mater. 41 (1971) 156.
[57] L.E. Thomas, in: S.E. Donelly, J.H. Evans (Eds.), Fundamental Aspects of Inert Gases in Solids, Plenum, New York, 1991, p. 431.
[58] K. Nogita, K. Une, Nucl. Instrum. and Meth. 91 (1994) 301.
[59] I.L.F. Ray, H. Thiele, Hj. Matzke, in: S.E. Donelly, J.H. Evans (Eds.), Fundamental Aspects of Inert Gases in Solids, Plenum, New York, 1991, p. 457.
[60] J.R. Matthews, G.J. Small, in: Proceedings of a Conference on Water Reactor Fuel Element Computer Modelling in Steady State, Transient and Accident Conditions, Preston, UK, 18–22 September 1988, p. 195, IWGFPT/32.
[61] H. Matzke, H. Blank, M. Coquerelle, K. Lassmann, I.L.F. Ray, C. Ronchi, C.T. Walker, J. Nucl. Mater. 166 (1989) 165.
[62] A.J. Manley, J. Nucl. Mater. 27 (1968) 216.
[63] M.E. Gulden, J. Nucl. Mater. 23 (1967) 30.
[64] R. Manzel, R.P. Bodmer, G. Bart, in: Proceedings of a Technical Committee Meeting, Pembroke, Ont., Canada, 28 April – 1 May 1992, IAEA-TECDOC-697, p. 63.
[65] R. Manzel, M. Coquerelle, M.R. Billaux, in: Proceedings of the International Topical Meeting on Light Water Reactor Fuel Performance, West Palm Beach, FL, USA, 17–21 April 1994, p. 335.
[66] T. Aoki, S. Koizumi, H. Umehara, K. Ogata, in: Proceedings of a Technical Committee Meeting, Pembroke, Ont., Canada, 28 April – 1 May 1992, IAEA-TECDOC-697, p. 44.
[67] M.R. Floyd, J. Novak, P.T. Truant, in: Proceedings of a Technical Committee Meeting, Pembroke, Ont., Canada, 28 April – 1 May 1992, IAEA-TECDOC-697, p. 53.
[68] H. Nerman, PM BK 83-118, AB Asea-Atom, Vesterås, Sweden, 83-04-11.
[69] R. Manzel, F. Sontheimer, R. Würtz, J. Nucl. Mater. 126 (1984) 132.
[70] M. Lippens, C. van Loon, J. Ketels, in: Proceedings of a Technical Committee Meeting on Properties of Materials for Water Reactor Fuel Elements and Methods of Measurements, Vienna, Austria, 13–16 October 1996, p. 69, IWGFPT/26.
[71] J. van Liet, in: Proceedings of a Technical Committee Meeting on Fuel Rod Internal Chemistry and Fission Products Behaviour, Karlsruhe, Germany, 11–15 November 1985, p. 96, IWGFPT/25.
[72] G. Lysell, S. Bengtsson, in: Proceedings of the International Topical Meeting on Light Water Reactor Fuel Performance, West Palm Beach, FL, USA, 17–21 April 1994, ANS, p. 301.
[73] F. Sontheimer, P. Dewes, R. Mantzel, H. Stehle, in: Proceedings of a Technical Committee Meeting in Karlsruhe, Germany, 11–15 November 1985, p. 108, IWGFPT/25.
[74] C.T. Walker, M. Coquerelle, in: Proceedings of the International Topical Meeting on LWR Fuel Performance, Avignon, France, 21–24 April 1991, ANS/ENS, p. 506.
[75] J. Rest, J. Nucl. Mater. 131 (1985) 291.
[76] J. Rest, in: Proceedings of a Technical Committee Meeting on Fuel Rod Internal Chemistry and Fission Products Behaviour, Karlsruhe, Germany, 11–15 November 1985, p. 131, IWGFPT/25.
[77] S. Ukai, T. Hosokawa, I. Shibahara, Y. Enokido, J. Nucl. Mater. 151 (1988) 209.
[78] I. Andersen, O. Grong, Acta Metall. 43 (7) (1995) 2673.
[79] D.R. Olander, Fundamental Aspects of Nuclear Reactor Fuel Elements, ERDA, USA, 1976, p. 314.
[80] T.J. Carter, I.J. Hastings, A.D. Smith, G.C. Miller, I.A. Lusk, R.E. Moeller, D.H. Rose, in: Proceedings of the International Topical Meeting on LWR Fuel Performance, Avignon, France, 21–24 April 1991, ANS/ENS, p. 818.
[81] M.E. Gunningham, D.D. Lanning, J.O. Barner, HBEP-50 (2P16), Battelle Northwest Laboratories, Richland, USA, 1987.
[82] P. Knudsen, C. Bagger, H. Carlsen, I. Misfield, M. Mogensen, Nucl. Technol. 72 (1986) 258.
[83] P. Knudsen, C. Bagger, H. Carlsen, B.S. Johansen, M. Mogensen, in: Proceedings of the American Nuclear Society Topical Meeting on LWR Fuel Performance, Williamsburg, VA, USA, 17–20 April 1988, p. 189.
[84] L.E. Thomas, R.J. Guenther, in: W. Lutze (Ed.), Proceedings of the International Symposium on Scientific Basis for Nuclear Waste Management XII, Pittsburgh, USA, Mater. Res. Soc. 127 (1989) 293.
[85] H. Ullmaier, in: S.E. Donelly, J.H. Evans (Eds.), Fundamental Aspects of Inert Gases in Solids, Plenum, New York, 1991, p. 277.
[86] G.W. Greenwood, A.J.E. Foreman, D.E. Rimmer, J. Nucl. Mater. 4 (1959) 305.
[87] H. Trinkhaus, Radiat. Eff. 78 (1983) 189.
[88] J.S. Lally, P.G. Partridge, Philos. Magn. 13 (1966) 9.
[89] W.R. Wampler, T. Schoeber, B. Lengeler, Philos. Magn. 34 (1976) 129.
[90] H. van Swijgenhoven, G. Knuyt, J. Vanoppen, L.M. Stal, Nucl. Instrum. and Meth. 209/210 (1983) 461.

[91] H. van Swijgenhoven, G. Knuyt, J. Vanoppen, L.M. Stal, J. Nucl. Mater. 114 (1983) 157.
[92] H. Trinkhaus, in: S.E. Donelly, J.H. Evans (Eds.), Fundamental Aspects of Inert Gases in Solids, Plenum, New York, 1991, p. 369.
[93] S.E. Donelly, D.R.G. Mitchell, A. van Veen, in: S.E. Donelly, J.H. Evans (Eds.), Fundamental Aspects of Inert Gases in Solids, Plenum, New York, 1991, p. 357.
[94] G.P. Tiwari, J. Singh, J. Nucl. Mater. 195 (1992) 205.
[95] P.J. Goodhew, in: S.E. Donelly, J.H. Evans (Eds.), Fundamental Aspects of Inert Gases in Solids, Plenum, New York, 1991, p. 349.
[96] J.H. Evans, J. Nucl. Mater. 61 (1976) 1.
[97] S.E. Donelly, Radiat. Eff. 90 (1985) 1.
[98] F.S. Ham, J. Phys. Chem. Solids 6 (1958) 335.
[99] A.J. Markworth, Mater. Sci. Eng. 10 (1972) 159.
[100] D.A. MacInnes, I.R. Brearley, J. Nucl. Mater. 107 (1982) 123.
[101] P.T. Elton, P.E. Coleman, D.A. MacInnes, J. Nucl. Mater. 135 (1985) 63.
[102] I.R. Breadley, D.A. MacInnes, J. Nucl. Mater. 118 (1983) 68.
[103] J. Rest, J. Nucl. Mater. 168 (1989) 243.
[104] C. Ronchi, J. Nucl. Mater. 148 (1987) 316.
[105] R.A. Jackson, C.R.A. Catlow, J. Nucl. Mater. 127 (1985) 167.
[106] J.H. Evans, A. van Veen, K.T. Westerduin, J. Nucl. Mater. 195 (1992) 250.
[107] C.C. Griffioen, J.H. Evans, P.C. de Jong, A. van Veen, Nucl. Instrum. and Meth. 27 (1987) 417.
[108] G.P. Tiwari, J. Singh, J. Nucl. Mater. 185 (1991) 224.
[109] A.D. Whapman, Nucl. Appl. 2 (1966) 123.
[110] A.M. Ross, J. Nucl. Mater. 30 (1969) 134.
[111] J.A. Turnbull, R.M. Cornell, J. Nucl. Mater. 36 (1970) 161.
[112] S.R. Pati, M.J. Dapht, D.R. O'Boyle, J. Nucl. Mater. 50 (1974) 227.
[113] G.J. Small, J. Nucl. Mater. 125 (1984) 117.
[114] C. Ronchi, P.T. Elton, J. Nucl. Mater. 140 (1986) 228.
[115] Ya.B. Zel'dovich, Yu.P. Raizer, Physics of Shock Waves and High-Temperature Hydrodynamic Phenomena, vol. II, Academic Press, New York, 1967.
[116] J.R. MacEwan, P.A. Morel, Nucl. Appl. 2 (1966) 158.
[117] L.C. Michels, R.B. Poeppel, J. Appl. Phys. 44 (3) (1973) 1003.
[118] W.M. Robertson, J. Nucl. Mater. 30 (1969) 36.
[119] J.H. Evans, A. van Veen, C.C. Griffioen, Nucl. Instrum. and Meth. B 28 (1987) 360.
[120] R.J. Cox, P.J. Goodhew, J.H. Evans, Nucl. Instrum. Meth. B 42 (1989) 224.
[121] E.E. Gruber, in: J.E. Harris, E.C. Sykes (Eds.), Proceedings of an international Conference on Physical Metallurgy of Reactor Fuel Elements, Gloucesterhire, UK, 2–7 September 1973, The Metals Society, 1975.
[122] P.J. Goodhew, J. Nucl. Mater. 98 (1981) 221.
[123] C. Ronchi, J. Nucl. Mater. 84 (1979) 55.
[124] H.R. Warner, F.A. Nichols, Nucl. Appl. Technol. 9 (1970) 148.
[125] F.A. Nichols, J. Nucl. Mater. 30 (1969) 143.
[126] K.H.G. Ashbee, Philos. Magn. 11 (1965) 637.
[127] W. Nixon, D.A. MacInnes, J. Nucl. Mater. 101 (1981) 192.
[128] C. Ronchi, C. Sari, J. Nucl. Mater. 50 (1974) 91.
[129] J.H. Evans, in: S.E. Donelly, J.H. Evans (Eds.), Fundamental Aspects of Inert Gases in Solids, Plenum, New York, 1991, p. 307.
[130] E.E. Gruber, Nucl. Technol. 35 (1977) 617.
[131] P.T. Sawbridge, C. Baker, R.M. Cornell, K.W. Jones, D. Reed, J.B. Ainscough, J. Nucl. Mater. 95 (1980) 119.
[132] F.A. Nichols, C. Ronchi, in: Proceedings of the International Conference on the Mobility of Fission Gas Bubbles in Fission-Product Behavior in Ceramic Oxide Fuel, vol. 17, American Ceramic Society,1986, pp. 85–93.
[133] J.H. Evans, J. Nucl. Mater. 246 (1997) 121.
[134] K. Une, S. Kashibe, J. Nucl. Sci. Technol. 27 (1990) 20.
[135] J.H. Evans, A. vanVeen, J. Nucl. Mater. 252 (1998) 156.
[136] G.P. Tiwari, J. Nucl. Mater. 252 (1998) 162.
[137] H. Schroeder, P.F.P. Fichtner, H. Trinkhaus, in: S.E. Donelly, J.H. Evans (Eds.), Fundamental Aspects of Inert Gases in Solids, Plenum, New York, 1991, p. 289.
[138] G.J. Small, in: Proceedings of the American Nuclear Society Topical Meeting on LWR Fuel Performance, Williamsburg, VA, USA, 17–20 April 1988, p. 278.
[139] J.A. Turnbull, J. Nucl. Mater. 62 (1976) 325.
[140] M.V. Speight, Nucl. Sci. Eng. 37 (1969) 180.
[141] R.J. White, M.O. Tucker, J. Nucl. Mater. 118 (1983) 1.
[142] W.J. Kilgour, J.A. Turnbull, R.J. White, A.J. Bull, P.A. Jackson, I.D. Palmer, in: Proceedings of the International Topical Meeting on LWR Fuel Performance, Avignon, France, 21–24 April 1991, ANS/ENS, p. 528.
[143] A. Denis, R. Piotrkowski, in: Proceedings of a Technical Committee Meeting, Windermere, UK, 19–23 September 1994, IAEA-TECDOC-957, p. 455.
[144] T. Nakajima, H. Saito, in: Proceedings of a Technical Committee Meeting on Water Reactor Fuel Behaviour and Fission Products Release in Off-Normal and Accident Conditions, Vienna, Austria, 10–13 November 1986, p. 140, IWGFPT/27.
[145] T. Nakajima, H. Saito, Nucl. Eng. Design 101 (1987) 267.
[146] M.R. Billaux, S.H. Shann, L.F. van Swam, F. Sontheimer, in: Proceedings of the International Topical Meeting on LWR Fuel Performance, Portland, OR, USA, 2–6 March 1997, ANS, p. 576.
[147] J. van Vliet, E. de Meulemeester, P. Bouffioux, Nucl. Eng. Design 56 (1980) 77.
[148] H. Nerman, in: Proceedings of a Conference on Water Reactor Fuel Element Computer Modelling in Steady State, Transient and Accident Conditions, Preston, UK, 18–22 September 1988, p. 567, IWGFPT/32.
[149] L.D. MacDonald, D.B. Duncan, B.J. Lewis, F.C. Iglesias, in: Proceedings of a Conference on Water Reactor Fuel Element Computer Modelling in Steady State, Transient and Accident Conditions, Preston, UK, 18–22 September 1988, p. 203, IWGFPT/32.
[150] D.D. Lanning, C.E. Beyer, G.A. Berna, K. Davis, in: Proceedings of the International Topical Meeting on LWR Fuel Performance, Portland, OR, USA, 2–6 March 1997, ANS, p. 601.
[151] M. Coquerelle, C. Ronchi, J. Sakellaridis, J. van de Laar, in: Proceedings of a Technical Committee Meeting on

Water Reactor Fuel Behaviour and Fission Products Release in Off-Normal and Accident Conditions, Vienna, Austria, 10–13 November 1986, p. 163, IWGFPT/27.
[152] C.T. Walker, K. Lassmann, C. Ronchi, M. Coquerelle, Nucl. Eng. Design 117 (1989) 211.
[153] T. Kogai, J. Nucl. Mater. 244 (1997) 131.
[154] M. Charles, J. Simmons, C. Lemaignan, in: Proceedings of a Conference on Water Reactor Fuel Element Computer Modelling in Steady State, Transient and Accident Conditions, Preston, UK, 18–22 September 1988, p. 221, IWGFPT/32.
[155] C. Ronchi, J. Sakellaridis, C. Syros, Nucl. Sci. Eng. 95 (1987) 282.
[156] W.H. Press et al., in: Numerical Recipes in FORTRAN, second ed., Cambridge University, Cambridge, 1994, ISBN 0-521-43064-X.